Production of quantum-degenerate mixtures of ytterbium and lithium with controllable interspecies overlap

Anders H. Hansen, Alexander Y. Khramov, William H. Dowd, Alan O. Jamison, Benjamin Plotkin-Swing, Richard J. Roy, and Subhadeep Gupta

Department of Physics, University of Washington, Seattle, Washington 98195, USA

(Received 12 November 2012; published 16 January 2013)

Quantum-degenerate mixtures of one-electron and two-electron atoms form the starting point for studying few- and many-body physics of mass-imbalanced pairs as well as the production of paramagnetic polar molecules. We recently reported the achievement of dual-species quantum degeneracy of a mixture of lithium and ytterbium atoms. Here we present details of the key experimental steps for the all-optical preparation of these mixtures. Further, we demonstrate the use of the magnetic field gradient tool to compensate for the differential gravitational sag of the two species and control their spatial overlap.

DOI: 10.1103/PhysRevA.87.013615 PACS number(s): 67.85.Pq, 37.10.De, 34.20.−b, 05.30.Fk

I. INTRODUCTION

Elemental quantum mixtures provide a path toward ultracold diatomic polar molecules [1]. Utilizing a second, distinguishable atomic species, such mixtures may also allow for impurity probing of quantum phenomena in an ultracold gas. Interspecies Feshbach resonances can enable studies of few- and many-body phenomena in mass-imbalanced systems. There has been great progress in the development of ultracold bi-alkali-metal gases, motivated by applications towards sympathetic cooling of Fermi gases [2], studies of strongly interacting mass-mismatched systems [3], and production of ultracold polar molecules [4].

Extending the choice of mixture components to include other parts of the periodic table, new scientific opportunities arise. For instance, the ground state of the diatomic molecule might now have a magnetic moment, leading to *paramagnetic* polar molecules. This has been a key motivation for our pursuit of the lithium-ytterbium combination.

The $^2\Sigma$ ground state of the YbLi molecule makes it a candidate system for simulating lattice spin models with applications in topological quantum computation [5]. Additionally, the Yb-Li mixture possesses a very large mass ratio, and a range of isotopic combinations with Bose and Fermi statistics. Tunable interactions between the components can lead to the creation of novel Efimov states [6]. When confined in an optical lattice, a heavy-light fermion mixture can realize the binary alloy model [7], with applications in simulating exotic condensed matter phases (e.g., studies of pattern formation [8,9]).

In previous work, we assessed the collisional stability of the Yb-Li mixture in weakly interacting regimes, and explored the strengths of various inelastic channels in a three-component mixture with one resonantly interacting pair. In this paper we describe the experimental details of our setup, stressing the areas that have required development beyond typical single-species experiments. We report on the production of large-number Bose- and Fermi-degenerate ytterbium gases and assess the cooling limits of the Yb-Li mixture from interspecies interactions. Finally we report the demonstration of interspecies spatial overlap control over a large temperature range, using a magnetic field gradient.

The remainder of this paper is organized as follows. In Sec. II we describe the salient features of our trapping apparatus. Section III discusses our atom manipulation and cooling techniques. In Sec. IV we summarize the performance of our system for the production of degenerate Yb-Li mixtures in different interaction regimes. Section V describes our interspecies spatial-overlap control scheme. Finally, in Sec. VI we present our conclusions and outlook.

II. TRAPPING APPARATUS

Our trapping apparatus uses standard techniques for single-species experiments, applied to two independent atomic sources, as pictured in Fig. 1. Yb and Li beams emerge from separate effusion ovens, and are directed towards the common "main" chamber through individually optimized Zeeman slower sections. The long slower tubes [lengths 93 cm (Li) and 40 cm (Yb), inner diameter 18 mm] also provide differential pumping. An additional stage of differential pumping is provided by a short tube (length 11 cm, inner diameter 5 mm) separating each oven assembly from an independently pumped "intermediate" chamber. We maintain the vacuum in each subchamber with ion pumps, and augment the main chamber vacuum with a titanium sublimation pump. During standard operation, the pressures are approximately $P_{\text{Li oven}} \simeq 3 \times 10^{-8}$ Torr, $P_{\text{Yb oven}} \simeq 1 \times 10^{-7}$ Torr, and $P_{\text{main}} < 1 \times 10^{-10}$ Torr, as measured by ion gauges. Each beamline is equipped with a gate valve, positioned between the oven and intermediate chambers. This allows us to perform single-species experiments, even when the other oven is being serviced.

A. Lithium and ytterbium ovens

The effusion ovens each consist of a vertically oriented "cup," connected via a 90° elbow to a nozzle: a 4-mm-diameter aperture in the Conflat (CF) assembly. We stabilize the Yb (Li) cup temperatures to 400 (375) °C during operation. The nozzles are stabilized at 450 °C permanently to prevent deposition and congestion. The areas between each nozzle and gate valve contain mechanical beam shutters mounted on rotary feedthroughs to control the atom flow to the main chamber, and a copper cold plate (−7 °C) to collect the atomic flux not directed towards the main chamber.

All heated oven parts are of type-316 stainless steel, while the rest of the vacuum apparatus is type-304 stainless steel.

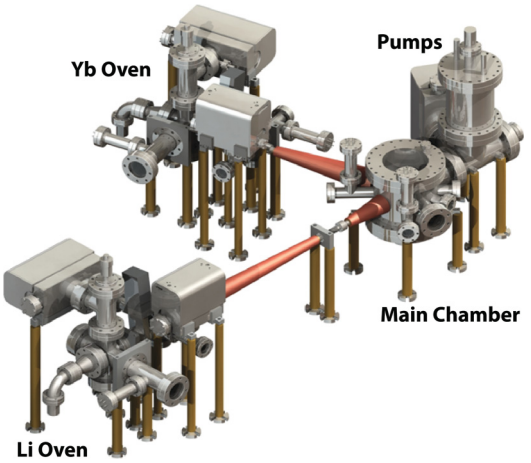

FIG. 1. (Color online) Schematic figure of dual-species apparatus. Ytterbium and lithium are prepared in separate ovens and slowed in individually optimized Zeeman slowers. Each oven is separated from the main chamber by two stages of differential pumping and an independently pumped intermediate chamber. The central part of each intermediate chamber (hidden from view) is a 2.75 in. six-way cross.

For the heated sections of the lithium oven we use nickel CF gaskets, which are more resilient than copper in high-temperature environments in the presence of lithium [10]. We have found, however, that nickel gaskets in the presence of hot Yb vapor undergo corrosive chemical reactions, which compromise the integrity of the vacuum after several months of operation. We now use copper gaskets in the ytterbium oven, which have been trouble-free for two years.

B. Main chamber

Our main chamber has a cylindrical geometry with ten viewports for optical access (Fig. 2). The top and bottom are sealed off by 10 in. CF flanges, into which custom-made re-entrant "buckets" for the electromagnets are recessed. Each bucket also has a 2.75 in. viewport for vertical MOT beams.

We keep the sapphire entry viewports for the Yb (Li) Zeeman slowing laser beams at a permanent 200 (250) °C; otherwise, metallic deposition is clearly evident. All other viewports are BK7 glass antireflection coated at the wavelengths for laser cooling and optical trapping of the two species.

Our experimental setup employs two pairs of electromagnetic coils, shown in Fig. 2. We apply antiparallel currents to the inner pair to generate the quadrupole field for the magneto-optical traps (MOTs), while the outer pair, arranged in parallel (Helmholtz) configuration, provide bias fields to access Feshbach resonances.

The MOT coils produce a vertical gradient of 1.0 G/cm/A, while the bias coils produce 4.2 G/A. We can electronically switch the MOT coils to parallel configuration, in which they yield 2.4 G/A . This allows for larger bias fields and improves the speed of magnetic field ramps.

Each coil is wound from hollow, square copper tubing (outer dimension 1/8 in., inner dimension 1/16 in.). A bias-field upper bound of 1000 G is set by the flow rate of the cooling water through the electromagnets at 100 psi building pressure.

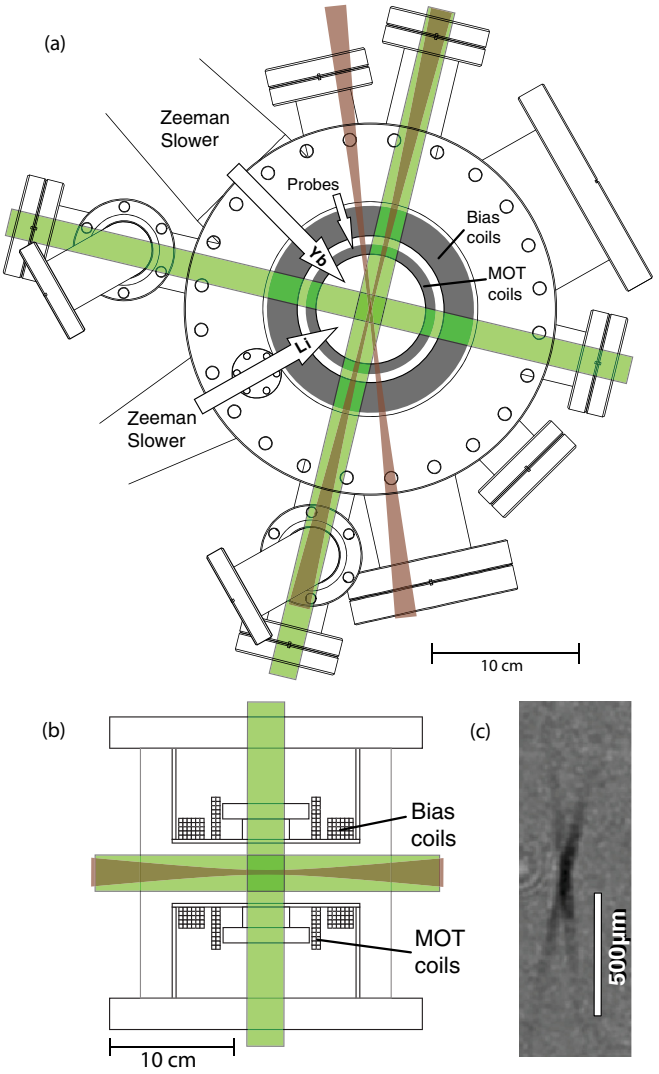

FIG. 2. (Color online) (a) Top view of main chamber, showing the configuration of magneto-optical trap (MOT) beams (green), optical dipole trap (ODT) beams (brown), magnetic coils (gray), and orientation of Yb and Li atomic beams and probe beams (arrows). Vertical MOT beams, vertical probe beams, slowing laser beams, and compensation coils are omitted for clarity. (b) Side view of main chamber, showing vertical and horizontal MOT beams, ODT beams, and recessed buckets with magnetic coils. (c) Sample in-trap absorption image of Yb atoms taken along the vertical axis, immediately after transfer to the ODT. The density distribution clearly shows the crossed-beam geometry. Upon further cooling, the atoms collect in the central crossing point of the two beams.

In order to reach higher fields (up to 1700 G), we employ a booster pump that raises the water pressure to 400 psi.

III. DUAL-SPECIES COOLING AND TRAPPING

We use three laser systems for slowing and laser cooling of lithium and ytterbium: one for ^{6}Li, addressing the $^2S_{1/2} \rightarrow {}^2P_{3/2}$ ($D2$) transition at 671 nm, and two for Yb, addressing the $^1S_0 \rightarrow {}^1P_1$ transition at 399 nm and $^1S_0 \rightarrow {}^3P_1$ (intercombination) transition at 556 nm (Fig. 3). We use acousto-optical modulators (AOMs) to provide all the required

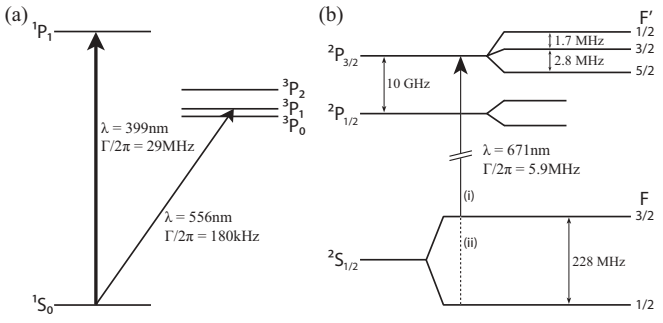

FIG. 3. Relevant energy levels for laser cooling of (a) ^{174}Yb and (b) ^{6}Li. Transitions used for trapping and cooling (see text) are indicated with arrows. In ^{173}Yb, only the excited states acquire hyperfine structure and the cooling lasers are tuned to the appropriate cycling transitions. To address lithium, we require separate frequency components for the cooling (i) and repumping (ii) transitions. The hyperfine splitting of the $^2P_{3/2}$ state is not resolved.

frequency shifts needed for slowing, trapping, repumping, and probing of the atoms.

We derive the 671 nm light from a commercial laser system (Toptica TA100), consisting of an external-cavity diode laser (ECDL) and a tapered amplifier (TA) system. We frequency-stabilize the laser using saturated absorption spectroscopy in a home-built vapor cell, with a lithium sample heated to 420 °C.

We derive the 399 nm light, used for slowing and imaging of Yb, from another commercial system (Toptica TA-SHG pro), consisting of an ECDL at 798 nm, a TA, and a second-harmonic generation (SHG) cavity. We frequency-stabilize this laser using saturated absorption spectroscopy in a commercial hollow-cathode lamp (Hamamatsu Laser Galvatron L2783).

We derive the 556 nm light, used for the Yb MOT, from another commercial system (Toptica FL-SHG pro), consisting of an ECDL, a fiber amplifier, and an SHG cavity. Since the linewidths of the blue and green transitions are different by more than two orders of magnitude, the two lasers require very different Yb column densities for spectroscopy. We frequency-stabilize this laser using saturated absorption spectroscopy in a home-built vapor cell with an ytterbium sample heated to 420 °C. In our setup, to reduce deposition on the cell viewports, we independently heat the viewport flanges while keeping the regions between the atomic sample and the glass at a lower temperature. We have also found it useful to reduce the diameter of the outermost section of the Yb cell on either end to reduce conduction.

A. Zeeman slowers

Each MOT loads from a separate Zeeman-slowed atomic beam. The solenoids for the Zeeman slowers are wound from the same copper wire as the MOT and bias coils. The Li slower uses a "spin-flip" configuration, consisting of a 60-cm-long decreasing-field section followed by a 15-cm-long increasing-field section. We operate each component at 30 A, yielding a net magnetic field variation $|\Delta\mathbf{B}|$ of 980 G. The atoms are slowed by a 40 mW laser beam, 732 MHz red-detuned from the $D2$ transition for the $F = \frac{3}{2}$ state. We derive the slower beam from an injection-locked diode laser. By adding a second injection beam 228 MHz blue-detuned from the first, we obtain light for repumping from the $F = \frac{1}{2}$ ground state within the slower.

The Yb slower consists of a single 40-cm-long increasing-field stage, operated at 15 A to yield $|\Delta\mathbf{B}| = 240$ G. The slowing beam has a power of 100 mW, and a red-detuning of 365 MHz from the $^1S_0 \rightarrow {}^1P_1$ transition.

Compensation coils, mounted opposite to each slower on the main chamber, cancel magnetic fringe fields at the position of the trapped atoms. Together with the vertical bias coils, the slower coils also serve as tools to move the center of the MOT quadrupole along all spatial axes, essential for relative positioning of the traps, as discussed below.

B. Magneto-optical traps

For magneto-optical trapping of the two species we use a standard single-species setup with retroreflected MOT beams [11], modified to accommodate a second atomic species. We combine the beams for the two species using a dichroic mirror, and divide the combined beam into three beams using broadband polarizing beam splitters. The polarizations are controlled by single-wavelength half-wave plates and dual-wavelength quarter-wave plates (Foctek).

Several factors have to be considered in determining the optimum parameters for dual-species laser cooling. Due to the difference in linewidth of the Li $D2$ and Yb intercombination lines (factor of 32) the two MOTs are optimized at very different magnetic gradients (see Table I). Furthermore, the optimal duration of the transitional cooling step (compression) before loading into the ODT differs greatly for the two species. Finally, the two species experience significant losses through inelastic collisions when the magneto-optical traps are spatially overlapped.

We find that the best performance in our setup is achieved using a sequential loading scheme, as described in [12], with typical parameters as listed in Table I. To summarize, we load Yb alone for 10–30 s, depending on experimental requirements. During this time, the detuning of the trapping light is modulated with an amplitude of 20 linewidths, at a frequency of 50 kHz, to increase the phase-space volume of the trapping region. We then compress Yb in 200 ms, and transfer it to the ODT. We subsequently optimize the

TABLE I. Typical experimental parameters for loading of ^{6}Li, ^{174}Yb, and ^{173}Yb: laser intensity I and red-detuning δ, and magnetic axial (vertical) field gradient B'. Two sets of numbers are provided for each isotope, reflecting the parameters for MOT loading and for the end point of compression (see the text) before transfer to the ODT. I refers to the total laser intensity in all three retroreflected beams; the total optical intensity at the atoms is twice the listed value. Γ and $I_{\rm sat}$ for Yb refer to the properties of the intercombination transition.

		^{6}Li $F = 3/2$	^{6}Li $F = 1/2$	^{174}Yb	^{173}Yb
Load	I	$60I_{\rm sat}$	$55I_{\rm sat}$	$750I_{\rm sat}$	$750I_{\rm sat}$
	δ	6Γ	3.5Γ	$(55 \pm 20)\Gamma$	$(40 \pm 20)\Gamma$
	B'	20 G/cm		3 G/cm	3 G/cm
Final	I	$0.07I_{\rm sat}$	$0.08I_{\rm sat}$	$0.8I_{\rm sat}$	$2I_{\rm sat}$
	δ	1.5Γ	3Γ	2Γ	4Γ
	B'	60 G/cm		18 G/cm	25 G/cm

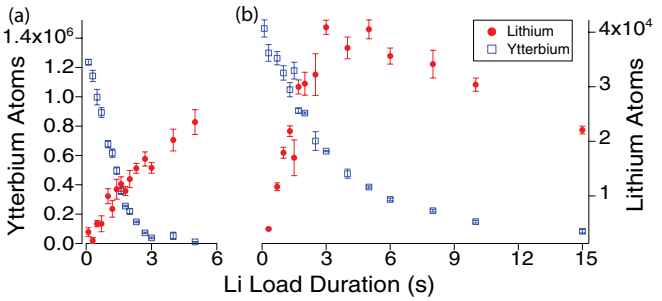

FIG. 4. (Color online) Number of trapped atoms, after a variable Li load time and 1 s hold in the ODT at fixed depth. (a) [(b)] shows results with a vertical bias field of 0 (2) G, corresponding to a 1 mm center-of-mass displacement of the Li MOT. In the favorably displaced case (b), Li numbers are optimized at a finite load time; at longer load times sympathetic cooling becomes inefficient due to low Yb numbers. Each error bar represents statistical fluctuations of four experimental iterations.

quadrupole field for lithium, load the Li MOT for 0.5–4 s (depending on experimental requirements), compress in 50 ms, and transfer to the ODT. A short (100 μs) pulse of light resonant with the Li $F = \frac{3}{2}$ $D2$ transition optically pumps the Li atoms into the ground $F = \frac{1}{2}$ state.

The positioning of the Li MOT during load is crucial for large dual-species samples as can be seen in Fig. 4. The large losses for suboptimal positioning can be interpreted as a consequence of elastic collisions that heat Yb through contact with the Li MOT, and also of inelastic collisions of ground-state Yb with electronically excited Li atoms in which both constituents are lost. The latter process also impedes the rate at which the Li MOT loads, as can be observed in Fig. 4.

We mitigate this effect by applying a bias field during the Li load, which spatially offsets the MOT from the ODT. With a vertical bias field of 2 G the lifetime of Yb atoms is quadrupled. Although this lifetime is less than the vacuum-limited lifetime of ∼45 s, this still leads to simultaneous confinement of 10^6 Yb atoms and 10^5 Li atoms in the ODT, immediately after switching off all the laser cooling beams.

Due to the greater abundance of Yb in the ODT, as well as its lower MOT temperature, Yb acts as a coolant for Li. At zero bias field we observe that, in the absence of Yb, most of the Li atoms spill from the trap during the first 1 s after transfer from the MOT. With a large bath of Yb present, these losses are mitigated, as the Li atoms thermalize with the bath.

C. Optical dipole trap

We derive our ODT from an ytterbium fiber laser (IPG Photonics YLR-100-LP) that can provide up to 100 W laser power at 1064 nm. During standard operation, we run the laser at 40 W. We send the laser output through an AOM and split the first-order output into two components of equal power and orthogonal polarization. Each component is focused to a waist of ≈26 μm and crossed at a 20° angle at the atoms. As shown in Fig. 2, both beams are horizontally aligned through the chamber. This configuration provides a straightforward geometry for our crossed ODT.

We perform evaporative cooling by controlling the efficiency of the ODT AOM. The geometry of the trap is thus preserved during evaporation, and trap frequencies may be interpolated between measurements at various depths [13].

D. Evaporative and sympathetic cooling strategies

For a given intensity of the 1064 nm ODT beam, the optical potential for Li is greater than that for Yb by a factor of about 2. Thus, at the same temperature, Yb will evaporate from the trap significantly faster than Li. For this reason, and because the Li (linear) size is smaller by a factor of 0.7 at equal temperature, the most practical cooling strategy involves sympathetically cooling Li in a bath of Yb. We thus optimize the initial conditions to a larger proportion ($\geqslant$90%) of trapped Yb, and set the rate of evaporative cooling to match the interspecies thermalization time, which is of order 1 s throughout. This method works well even in the regime of quantum degeneracy, since the condensation temperature for Yb is an order of magnitude lower than the Li Fermi temperature (for equal Li and Yb numbers). A more detailed discussion of this scheme can be found in [14].

We believe that this method of cooling will readily transfer to other alkali metal + spin-singlet systems, where some performance aspects may be even better than in Yb-Li. The number of interspecies collisions necessary for thermalization between particles of masses m_1 and m_2 is of order $2.7/\xi$, where the dimensionless parameter $1/\xi = (m_1 + m_2)^2/4m_1m_2$ [15]. For ^{6}Li and ^{174}Yb, $2.7/\xi = 21$, which is relatively large. Furthermore, since Li cannot be laser cooled to such low temperatures as Yb, a considerable amount of Yb is lost through evaporation during initial thermalization. Both of these effects will be less severe with other alkali-metal atoms such as Na, K, Rb, and Cs. We also note that a similar mismatch of trap depth in a 1064 nm ODT will exist and a similar immunity to two-body inelastic losses is expected, both advantageous for sympathetic cooling with Yb [16].

E. Simultaneous dual-species imaging

We simultaneously probe the collocated, optically trapped clouds of Li and Yb using absorption imaging. The imaging beams are overlapped before they enter the vacuum chamber, using a broadband polarizing beam splitter. The beams are split after they emerge from the vacuum chamber using dichroic mirrors, and the cloud images are projected onto two different regions of the CCD camera chip. Absorption images for both clouds are obtained for each experimental iteration.

IV. Yb-Li QUANTUM MIXTURES

Our quantum mixture preparation relies on the direct evaporative cooling of Yb which then cools the co-trapped Li sympathetically, as described in Sec. III D. Cooling in the absence of an external magnetic field leads to weakly interacting Bose-Fermi mixtures. By applying external magnetic fields, strongly interacting regimes may then be accessed through available Feshbach resonances. In this section, we first report our current system performance for producing quantum-degenerate gases of single-species Yb isotopes. We then present the production of weakly interacting Yb-Li mixtures through sympathetic cooling. Finally we briefly discuss regimes of strong interactions in Yb-Li mixtures.

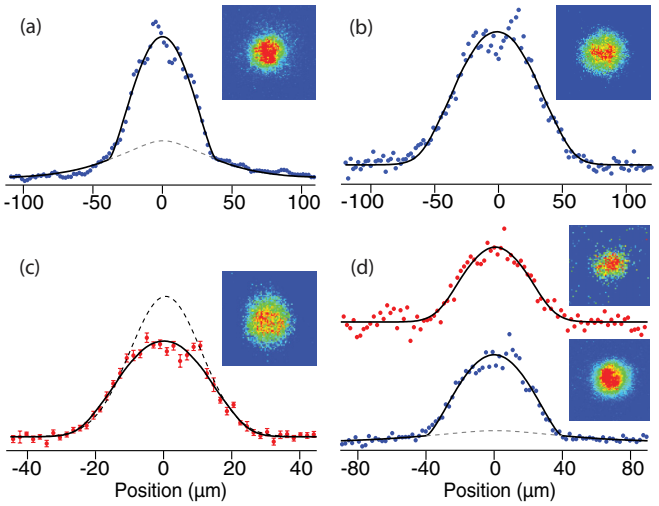

FIG. 5. (Color online) Density cross sections of lithium and ytterbium from absorption images (insets) of degenerate gases. (a) Quantum-degenerate gas of ^{174}Yb atoms with 2.5×10^5 atoms in the condensate imaged at a time of flight (TOF)12 ms. (b) Degenerate Fermi gas of 1×10^5 ^{173}Yb atoms with $T/T_F = 0.3$ and TOF 5 ms. (c) Degenerate Fermi gas of 1.6×10^4 ^{6}Li atoms with $T/T_F \approx 0.06$ and TOF 0.4 ms. (d) Simultaneous quantum degeneracy of ^{6}Li and ^{174}Yb with 2×10^4 (3×10^4) atoms of Li (Yb). $T/T_F \approx 0.2$ for Li and TOF 0.5 (10) ms. Solid lines are least-square fits to local-density-approximation models for Bose and Fermi gases, while dashed lines are classical fits to the wings of the distributions.

A. Quantum-degenerate ytterbium

Our current apparatus has several new features beyond what was reported in [14]. Our Yb laser cooling procedure now employs greater power and frequency sweep range in the MOT beams during load (see Sec. III). The optical trap now features electronic stabilization of depth and adjustable volume through a time-averaged potential generated by frequency modulation of the ODT AOM [18]. This "painting" of the potential increases the volume of the loading trap and allows a much larger load of Yb. Optimization of both loading and evaporation is obtained by continuously reducing the volume and the depth of the trap during evaporative cooling. Loading from 7×10^7 laser-cooled atoms at a temperature of $\simeq$20 μK, we achieve an optical trap load of up to 5×10^6 atoms and ^{174}Yb condensate numbers of 3×10^5 [Fig. 5(a)]. Applied to fermionic ^{173}Yb, we can achieve up to 1.2×10^5 [Fig. 5(b)] atoms in a mixture of the six spin states at $\frac{T}{T_F} = 0.3$. By reducing the loading and evaporative cooling sequence times, we can improve the repetition rate of Yb condensate production to 10 s, with (5×10^4)-atom Bose-Einstein condensates (BECs). Fast experimental repetition rates are crucial to precision measurements with BECs, which depend on large statistical data samples [19].

B. Weakly interacting quantum-degenerate Yb-Li mixture

For dual-species experiments in which Li is co-trapped and sympathetically cooled by Yb, the time-averaging option is not used as the accompanying reduction in trap depth is too great to efficiently load Li into the optical trap. As noted earlier, the larger polarizability of Li makes Yb a suitable sympathetic coolant. At the lowest temperatures, the large mass difference affects the standard procedure in two significant ways—the degeneracy temperatures for equal numbers are different by an order of magnitude, and the differential gravity-induced trap modification is relatively large.

By controlling the final depth of the evaporation ramp, we achieve simultaneous degeneracy, with similar atom numbers (few $\times 10^4$) of each species. The quantum-degenerate Yb-Li mixture at zero external magnetic field [Fig. 5(d)] is weakly interacting with interspecies scattering length of magnitude $13a_0$ [12,14,20]. In our system, $N_{\rm Li} \approx N_{\rm Yb}$ when the condensation temperature T_C is achieved. By this stage of the cooling the volume of the Li Fermi gas (constrained by Fermi degeneracy) is larger than that of the coolant Yb bosons. The reduction in size and heat capacity of the coolant, and the differential gravitational sag are all effects which can reduce the sympathetic cooling efficiency [14]. Further, we might expect a reduction in condensate number in the presence of Li, due to collisions between energetic Li atoms near the Fermi velocity $v_F \simeq 5$ cm/s and the Yb BEC (peak condensate speed of sound $v_c \simeq 1$ mm/s), which may explain the condensate number reduction reported in [20].

In spite of the aforementioned issues, sympathetic cooling can produce deeply degenerate Fermi gases in our apparatus. By sacrificing all of the coolant Yb through evaporation, temperatures below $0.1T_F$ can be achieved [Fig. 5(c)]. By keeping a small amount of Yb in the trap, we establish a system in which Yb may act as an impurity probe of the ^{6}Li degenerate Fermi gas.

C. Yb-Li mixtures in strongly interacting regimes

Two different regimes of strong interactions in the Yb-Li system are of current scientific interest. The first one is a three-component system of Yb and two resonantly interacting Li spin states, a regime recently explored experimentally by Khramov *et al.* [21]. Here studies of strongly interacting Fermi gases using Yb as a dissipative bath or an impurity probe may be carried out. While the strong interactions induce inelastic loss processes at unitarity, which are unobservable in the weakly interacting regime, the interspecies elastic processes still dominate and we have observed temperatures as low as $0.25T_F$.

The other strongly interacting regime of current interest is a Feshbach resonance between Yb and Li atoms. Theoretical calculations by Brue and Hutson [22], predict narrow magnetically induced Feshbach resonances between ^{173}Yb and ^{6}Li. These have not yet been experimentally observed.

A fundamental limiting factor in preserving interspecies contact in degenerate Yb-Li mixtures is the differential gravitational sag of the two species at low trap depths. In our trap, the Yb atoms, due to their greater mass and weaker optical confinement, become significantly displaced from the Li atoms at temperatures near 300 nK, compromising the efficiency of sympathetic cooling and generally the study of any interspecies interaction effects. A technique for circumventing this limitation is discussed in the following section.

V. CONTROL OF INTERSPECIES SPATIAL OVERLAP

Differences in internal properties between components of an ultracold mixture can result in a differential response to external fields. This sometimes leads to unwanted effects such as the differential vertical displacement due to gravity experienced in mixtures with unequal mass constituents. For the weak optical potentials needed to achieve the highest phase-space densities, this "gravitational sag" leads to reduced spatial overlap and reduced interspecies interactions. The differential gravitational sag is an important limiting factor for the molecule formation efficiency in the K-Rb mixture [23], where the mass ratio is 2.2. In the case of the Yb-Li mixture, where the mass ratio is 29, this effect is even more significant, leading to a nearly complete decoupling of the two species at the lowest temperatures [14]. Here we demonstrate that this differential gravitational sag can be mitigated by the use of a magnetic field gradient which exerts a force on only the lithium component.

In principle, one may use external magnetic fields to achieve independent control of any two atomic species. For instance, in alkali-metal atoms with half-integer nuclear spin there will exist states with magnetic projection $m_F = 0$ in the direction of the magnetic field, allowing one species to be made insensitive to magnetic gradients. However, this insensitivity does not extend to the high magnetic fields often required in experiments (e.g., to address Feshbach resonances) due to hyperfine decoupling. Furthermore, mixtures of high-field- and low-field-seeking atoms are prone to inelastic, internal state-changing collisions, which lead to trap losses.

Mixtures of alkali-metal and alkaline-earth-metal atoms avoid these limitations as the ground-state magnetic moment of the alkaline-earth-metal species is zero or nearly zero for all external fields. Furthermore, in isotopes with zero nuclear moment, spin-exchange collisions are suppressed entirely. This feature has been used to overlap clouds of magnetically trapped rubidium atoms with optically trapped ytterbium atoms [24]. Here we report on manipulating the relative displacement of two species that are confined in the same optical trapping potential, and over a large temperature range down to <1 μK.

When atoms in a trap are subjected to a uniform force $F = mg$, the center of mass is displaced by an amount $\Delta z = g/\omega^2$, where ω is the vertical trapping frequency. Due to differences in mass and polarizability, the trap frequencies for Li and Yb differ by a factor of 8, leading to substantial differential gravitational sag at low trap depths.

We demonstrate control of interspecies spatial overlap by applying a magnetic gradient which acts as a "pseudogravitational" force on Li only. We first prepare a mixture of ^{6}Li in its two lowest-energy states and the single ground state of ^{174}Yb at a particular optical trap depth. For experimental simplicity, we ramp the bias field to 530 G, where the two Li spin states have equal magnetic moments $1\mu_B$ and negligible interaction strength. We then turn on our MOT coils to add a magnetic quadrupole field to the vertical bias field, thereby creating a magnetic force in the direction of the bias field. Our system is capable of producing vertical gradients up to 170 G/cm; however, a more modest gradient of 65 G/cm is sufficient to make the atom clouds concentric.

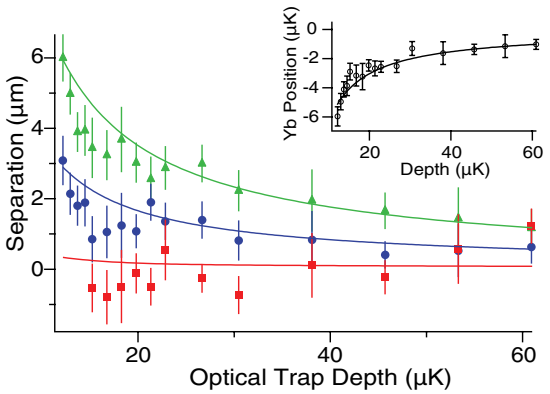

FIG. 6. (Color online) Relative displacement of centers of mass of Li and Yb clouds, versus optical trap depth for Yb atoms, at various magnetic gradients: -13 G/cm (filled triangles), 35 G/cm (filled circles), and 64 G/cm (filled squares). Each data point gives the average center-of-mass position of between 7 and 12 absorption images of lithium, subtracted from the average of 11 ytterbium images. The inset shows the displacement of Yb from the ODT beam center. The solid lines are results of a numerical model.

Figure 6 shows the separation of the cloud centers as a function of optical potential for different magnetic gradients. The gradient strength was determined by releasing the Li atoms and imaging them after a variable time to measure the acceleration $\mu_B B'/m_{\mathrm{Li}} + g$. The analysis also identified and corrected for slight ($<1^\circ$) deviations of the long trap axis from horizontal and the magnetic bias from vertical.

The lowest Yb optical trap depth for the data in Fig. 6 is 12 μK. Due to gravity, this corresponds to an effective trap depth of 4 μK, which goes to zero at an optical trap depth of 6 μK. We observe the onset of BEC at 15 μK optical depth when loading Yb alone.

At the lowest depths, the in-trap $1/e$ height of the ytterbium cloud is approximately 2 μm, whereas the Li cloud size is near the Fermi radius of 6 μm. Thus, in the absence of a magnetic gradient, the spatial overlap of the two clouds is critically reduced at trap depths below 20 μK.

Also shown in Fig. 6 is a set of theoretical curves of relative displacement, derived from a simple numerical model assuming a Gaussian trap profile. The only variable parameter in the model is the ODT (vertical) beam waist, which agrees at the 10% level with measurements of trap frequency via parametric excitation. We find reasonably good agreement between this model and the experimental data, although the calculation slightly overestimates the degree of sag at the lowest trap depths. One plausible explanation for this is a small vertical misalignment of the ODT beams, leading to a deviation from a Gaussian profile.

A side effect of this technique is that the applied gradient, while shifting the center of the trap, also effectively lowers the trap depth. Thus, for deeply degenerate Fermi clouds where the initial trap depth is close to the Fermi temperature, the "tilted" potential leads to spilling of Li atoms near the Fermi energy. This effect appears as a gradient-dependent Li number loss at

the lowest depths (when $T \lesssim 0.1T_F$) in our experiment and has been utilized elsewhere to measure interaction strength in Fermi gases [25] and to accelerate evaporative cooling in Bose gases [26].

We also note that the field inhomogeneity introduced by the magnetic gradient can limit its usefulness in experiments that require extremely homogeneous magnetic fields. For instance, a gradient of 65 G/cm corresponds to a magnetic field variation of tens of milligauss across the sample, much larger than the theoretical width of the predicted magnetic Feshbach resonances between ^{173}Yb and ^{6}Li [22].

Species-selective control of atomic samples has also been demonstrated using only optical fields. Bichromatic optical traps exploiting the different ac Stark shifts of atoms have been demonstrated [24]. Our technique has the advantage of requiring no additional lasers or sensitive alignment of optics. The effect is achieved entirely with existing hardware, operating under typical conditions.

In addition to the application described above, the magnetic gradient technique enables experiments involving the use of one atomic species as a local probe of the other. In the ^{6}Li-^{174}Yb system, the Yb acts as a "bath" at temperatures above degeneracy, where its cloud is much larger than that of Li. At low temperatures, Yb can act as a "probe," since the Yb cloud is much smaller than the Li Fermi radius [21]. Under the latter conditions, Yb can be a useful probe for studying the local properties of a Fermi gas in the weakly interacting as well as in the superfluid regime.

Beyond spatial control, one can also use magnetic gradients to achieve selective control of the momentum of the magnetically sensitive species, by changing the gradient nonadiabatically. Such velocity-control techniques may be useful for a range of studies, such as measures of viscosity and tests of superfluidity.

VI. CONCLUSIONS AND OUTLOOK

We have presented a detailed description of our apparatus to produce stable quantum mixtures of lithium and ytterbium atoms. We have also demonstrated a method of controlling the spatial overlap of the two species, general to combinations of magnetic and nonmagnetic atoms. When prepared near the ^{6}Li Feshbach resonance, bosonic Yb can act as a microscopic probe of the strongly interacting lithium Fermi gas. Other future applications of the mixture include the study of condensed matter models in an optical lattice, such as the binary-alloy model.

An interspecies Feshbach resonance between lithium and ytterbium will allow the exploration of three-body Efimov states with large mass mismatch, and potential studies of the many-body physics of mass-imbalanced pairs. While such resonances have not yet been observed, they may show up in the near future in experiments with the ground-state mixture, or by using Yb in an excited metastable state (such as $^{3}P_2$) [27]. An additional possibility is an interspecies optical Feshbach resonance [28]. Finally, the quantum-degenerate mixture of lithium and ytterbium provides the starting point for the production of quantum gases of paramagnetic polar molecules of YbLi. Such ultracold molecules are of general interest from the perspective of quantum simulation [5], quantum information [29], tests of fundamental symmetries [30], and probes of time variations of physical constants [31].

ACKNOWLEDGMENTS

We thank Lee Willcockson and Ryan Weh for major technical contributions during the early stages of the experiment. This work was supported by the National Science Foundation, the Air Force Office of Scientific Research, the Alfred P. Sloan Foundation, the UW Royalty Research Fund, and NIST.

[1] L. D. Carr, D. DeMille, R. V. Krems, and J. Ye, New J. Phys. **11**, 055049 (2009).
[2] Z. Hadzibabic, C. A. Stan, K. Dieckmann, S. Gupta, M. W. Zwierlein, A. Görlitz, and W. Ketterle, Phys. Rev. Lett. **88**, 160401 (2002).
[3] C. Kohstall, M. Zaccanti, M. Jag, A. Trenkwalder, P. Massignan, G. M. Bruun, F. Schreck, and R. Grimm, Nature (London) **485**, 615 (2012).
[4] K.-K. Ni, S. Ospelkaus, M. H. G. de Miranda, A. Peer, B. Neyenhuis, J. J. Zirbel, S. Kotochigova, P. S. Julienne, D. S. Jin, and J. Ye, Science **322**, 231 (2008).
[5] A. Micheli, G. K. Brennen, and P. Zoller, Nat. Phys. **2**, 341 (2006).
[6] E. Braaten and H. W. Hammer, Phys. Rep. **428**, 259 (2006).
[7] C. Ates and K. Ziegler, Phys. Rev. A **71**, 063610 (2005).
[8] M. M. Maska, R. Lemanski, J. K. Freericks, and C. J. Williams, Phys. Rev. Lett. **101**, 060404 (2008).
[9] M. M. Maska, R. Lemanski, C. J. Williams, and J. K. Freericks, Phys. Rev. A **83**, 063631 (2011).
[10] C. A. Stan and W. Ketterle, Rev. Sci. Instrum. **76**, 063113 (2005).
[11] H. J. Metcalf and P. Van der Straten, *Laser Cooling and Trapping* (Springer, Berlin, 1999).
[12] V. V. Ivanov, A. Khramov, A. H. Hansen, W. H. Dowd, F. Münchow, A. O. Jamison, and S. Gupta, Phys. Rev. Lett. **106**, 153201 (2011).
[13] At the highest laser powers (>50 W), however, we have observed thermal lensing effects in various optical components in the ODT path.
[14] A. H. Hansen, A. Khramov, W. H. Dowd, A. O. Jamison, V. V. Ivanov, and S. Gupta, Phys. Rev. A **84**, 011606(R) (2011).
[15] A. Mosk, S. Kraft, M. Mudrich, K. Singer, W. Wohlleben, R. Grimm, and M. Weidemüller, Appl. Phys. B: Lasers Opt. **73**, 791 (2001).
[16] Three-body losses may then be the dominant loss mechanism, as in the ^{174}Yb-^{87}Rb mixture [17].
[17] F. Baumer, F. Münchow, A. Görlitz, S. E. Maxwell, P. S. Julienne, and E. Tiesinga, Phys. Rev. A **83**, 040702(R) (2011).
[18] K. Henderson, C. Ryu, C. MacCormick, and M. Boshier, New J. Phys. **11**, 043030 (2009).
[19] A. O. Jamison, J. N. Kutz, and S. Gupta, Phys. Rev. A **84**, 043643 (2011).

[20] H. Hara, Y. Takasu, Y. Yamaoka, J. M. Doyle, and Y. Takahashi, Phys. Rev. Lett. **106**, 205304 (2011).
[21] A. Y. Khramov, A. H. Hansen, A. O. Jamison, W. H. Dowd, and S. Gupta, Phys. Rev. A **86**, 032705 (2012).
[22] D. A. Brue and J. M. Hutson, Phys. Rev. Lett. **108**, 043201 (2012).
[23] J. J. Zirbel, K.-K. Ni, S. Ospelkaus, J. P. D'Incao, C. E. Wieman, J. Ye, and D. S. Jin, Phys. Rev. Lett. **100**, 143201 (2008).
[24] S. Tassy, N. Nemitz, F. Baumer, C. Höhl, A. Batar, and A. Görlitz, J. Phys. B **43**, 205309 (2010).
[25] S. Jochim, M. Barternstein, A. Altmeyer, G. Hendl, S. Riedl, C. Chin, J. Hecker Deschlag, and R. Grimm, Science **302**, 2101 (2003).
[26] C.-L. Hung, X. Zhang, N. Gemelke, and C. Chin, Phys. Rev. A **78**, 011604(R) (2008).
[27] S. Kato, S. Sugawa, K. Shibata, R. Yamamoto, and Y. Takahashi, arXiv:1210.2483.
[28] S. Blatt, T. L. Nicholson, B. J. Bloom, J. R. Williams, J. W. Thomsen, P. S. Julienne, and J. Ye, Phys. Rev. Lett. **107**, 073202 (2011).
[29] D. DeMille, Phys. Rev. Lett. **88**, 067901 (2002).
[30] J. J. Hudson, D. M. Kara, I. J. Smallman, B. E. Sauer, M. R. Tarbutt, and E. A. Hinds, Nature (London) **473**, 493 (2011).
[31] M. Kajita, G. Gopakumar, M. Abe, and M. Hada, Phys. Rev. A **84**, 022507 (2011).